Ionics (2008) 14:279–283
DOI 10.1007/s11581-007-0179-7

ORIGINAL PAPER

Structural, magnetic and redox properties of a new cathode material for Li-ion batteries: the iron-based metal organic framework

C. Combelles · M.-L. Doublet

Received: 3 September 2007 / Accepted: 29 October 2007 / Published online: 25 November 2007
© Springer-Verlag 2007

Abstract The iron-based metal organic framework (MOF) presently studied is the first example of MOF showing a reversible electrochemical Li insertion with a very good cycling life. Its potential application as a cathode material in Li-ion battery is nevertheless curbed by a rather poor capacity of 70 mAh/g. To figure out the origin of this limited insertion, first-principles density functional theory (DFT)+U calculations were performed. The results show that Fe^{III}{OH(BDC)} is a weak anti-ferromagnetic charge transfer insulator at T=0 K with iron in the high-spin S=5/2 state. In agreement with the absence of electronic delocalisation along the inorganic chains, lithium insertion leads to the stabilisation of a Fe^{II}/Fe^{III} mixed-valence state of class I or II in the Robin–Day classification, whatever the Li sites considered in the calculations. Among these Li sites, the most probable site I (OH-Li) and site II (O=CO-Li) are shown to induce incompatible structural changes on the reduced $Li_{0.5}$Fe{OH(BDC)} form that could be at the origin of the small capacity measured for this compound.

Keywords First-principles DFT · Cathodes · Li-ion batteries · Magnetism · Mixed-valence

Introduction

Metal organic frameworks (MOFs) are new functional materials that combine a wide variety of properties and applications. They contain inorganic and organic networks that can be easily functionalised to get tuneable properties. Commonly used in sensing, catalysis, ion exchange, separations or gas storage [1–7], they have recently been thought as possible candidates for applications in lithium energy storage (Li-ion batteries) [8–9]. The interest of using such open-space frameworks for Li-Ion battery applications relies on an expected increase of the kinetics of lithium diffusion, which is one of the major limitation of dense electrodes. Among them, the iron-based Fe{OH(BDC)} (BDC-O_2C-C_6H_4-CO_2-benzodicarboxylate) compound was recently tested as a cathode material in a Li-ion battery cell [9]. Its electrochemical activity with respect to elemental lithium has shown interesting performances, such as good cycling life and rate capability. Unfortunately, the material suffers from a rather poor capacity of about 70 mAh/g, associated with the insertion of at most 0.5 Li per iron atom. This is half the capacity of the commonly used $LiCoO_2$ [10] or olivine $LiFePO_4$ cathode materials [11]. These first attempts are nevertheless encouraging because the number of inserted lithium could be, in principle, increased up to one Li per transition metal (TM), i.e. one electron per TM, thus doubling the capacity of the material. In the present case of Fe{OH(BDC)}, it would correspond to the reduction of all iron ions from the +III to the +II oxidation state, instead of one every iron. To this goal, one has first to figure out the origin of this limited lithium insertion in elucidating the electronic structure of the system.

First-principles density functional calculations have proven to be powerful in predicting the thermodynamic, structural and electronic properties of a wide series of solids, especially in the field of lithium energy storage [12–15]. It is also well admitted that variants of the standard density functional theory (DFT) such as the self-interaction DFT+U [16, 17] methods are required to properly account for the electron correlation in dense

Paper presented at the 11th EuroConference on the Science and Technology of Ionics, Batz-sur-Mer, Sept. 9–15, 2007.

C. Combelles · M.-L. Doublet (✉)
Institut Charles Gerhardt, CNRS-UMII-ENSCM-UMI,
Université Montpellier II,
Place Eugène Bataillon,
34095 Montpellier Cedex 5, France
e-mail: marie-liesse.doublet@univ-montp2.fr

transition metal oxides [18–20] or rare earth-based systems [21]. In this method, non-integer or double occupations of the 3*d* electronic levels are penalised by the introduction of two additional interaction terms, namely, the one-site Coulomb interaction term U and the exchange interaction term J, by means of an effective parameter $U_{eff}=U-J$. This approach was then used to investigate the electronic structure of the $Li_xFe\{OH(BDC)\}$ ($x=0$ to 1). The structural, magnetic and redox properties were then studied as a function of U_{eff}, varying from the DFT limit ($U=0$) to the strongly correlated limit ($U_{eff}=9$ eV).

Computational details

Calculations were performed using the plane wave DFT code from the Vienna ab initio simulation package (VASP) [22, 23] within the DFT+U formalism [16, 17] using the Liechtenstein method [24] with $J=1$ eV. For the sake of comparison, all observables were computed from the DFT limit ($U=0$) to the strongly correlated limit ($U_{eff}=9.0$ eV) within both the local density approximation (LDA) [25] and the generalised gradient approximation of Perdew–Burke–Erzenhorf (GGA-PBE) [26, 27] for the exchange and correlation potentials. The electron wave functions were described in the projected augmented wave formalism (PAW) [28] and a real-space projection was further used for the total wave function analyses. The plane wave energy cut-off was set up to 1000 eV, and a value of 600 eV was chosen as the default parameter. The Brillouin zone integration was done in a k-point grid as uniformly distributed as possible, using a 5×3×5 Monkhorst–Pack mesh (38 irreducible k-points) for structural relaxations and a 7×5×7 (123 irreducible k-points) for density of states and band structure analyses. The ionic convergence was done with respect to both the atomic forces (less than 3.10^{-3}) and the energies (less than 10^{-5}).

Results

The Fe{OH(BDC)} system crystallises in the $C_{2/c}$ space group ($a=6.882$ Å, $b=21.249$ Å, $c=6.763$ Å, $\beta=114.62°$) whose primitive unit cell is indexed in the P_{-1} space group ($a=6.882$ Å, $b=11.150$ Å, $c=6.763$ Å, $\beta=107.7°$, $\gamma=113.4°$). As shown Fig. 1, the structure is described by chains of corner-shared FeO_6 distorted octahedra running along the a-axis, and connected to each other through benzo-dicarboxylate (BDC) organic linkers in the b-direction. Such BDC packing yields a π-like stacking along the c-axis. Two iron atoms occur in each chain. They are bonded to six oxygen atoms belonging to two bridging hydroxo (OH) groups for the apical ligands and two bidentate carboxylate groups for the equatorial ligands. This leads to distorted FeO_6 octahedra, described by two short Fe-OH apical bonds ($2x$ Fe-O_a=1.964 Å), and four longer Fe-OC equatorial bonds (2 × Fe-O_e=2.012 Å and 2 × Fe-O_e=2.112 Å).

Table 1 reports the experimental and computed lattice parameters, bond distances and equilibrium volumes for the Fe{OH(BDC)} system, obtained from full structural relaxations for various U_{eff} from the DFT limit ($U=0$) to the strongly correlated limit ($U_{eff}=9$ eV).

As often reported in dense transition metal oxides [18–20], the bond lengths and, therefore, the lattice parameters are slightly overestimated compared to experiments, whilst no significant variations result from the increase of U_{eff}. It is surprising to note that the c-lattice parameter is also well reproduced by the calculations although weak Van der Waals interactions occur in that direction. A very small dependence of the total energy is, however, obtained with respect to the increase of the c-lattice parameter, consistent with a very low c-compressibility. The LDA leads to equivalent results for the c-lattice parameter. Nevertheless, as shown in Fig. 2, both the Fe-O bonds and the lattice parameters are underestimated, in full agreement with the well-known feature of LDA to overestimate binding

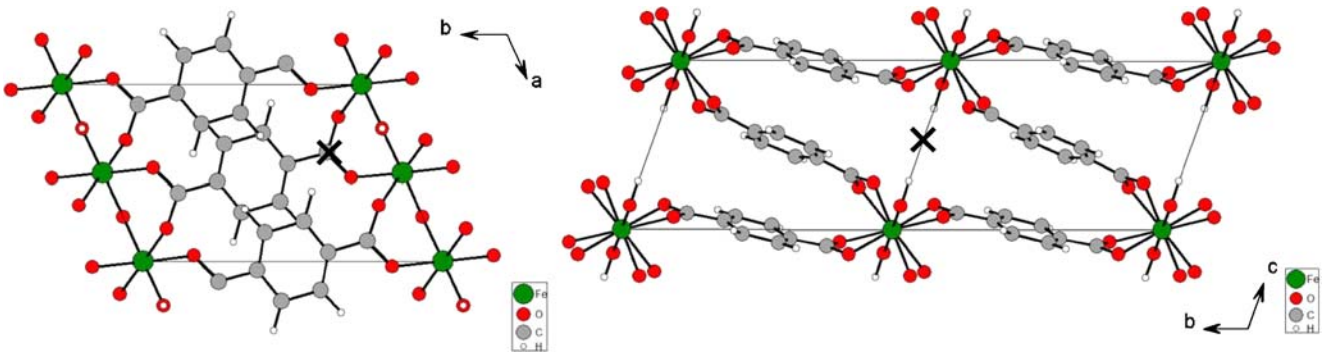

Fig. 1 Crystal structure of Fe{OH(BDC)} (P_{-1} space group) projected in the (a, b) and (b, c) planes, the chains of FeO_6 octahedra running along the a-axis. Iron, oxygen and carbon atoms are illustrated by *green*, *red* and *grey circles*, respectively. The most probable Li sites are given by *crosses*

Table 1 Lattice parameters, unit cell volume Ω, Fe-O bond distances and iron local magnetic moments (μ_{Fe}) for the neutral Fe{OH(BDC)} compound computed within the GGA-PBE functional for various U_{eff} values from the DFT limit (U=0) to the strongly correlated one (U_{eff}=9 eV)

	U_{eff} (eV)=U-J with J=1 eV						
	Exp	0	2	4	5	7	9
a (Å)	6.882	6.981	7.008	7.008	7.006	6.977	6.916
b (Å)	11.150	11.238	11.241	11.247	11.229	11.206	11.192
c (Å)	6.763	6.814	6.813	6.914	6.882	7.002	6.989
Ω	449.6	462.9	471.4	472.0	469.7	475.4	469.1
Fe-O_a (Å)	1.964	1.961	1.979	1.979	1.977	1.969	1.949
Fe-O_e (Å)	2.012	2.028	2.021	2.025	2.021	2.014	1.996
Fe-O_e (Å)	2.112	1.066	2.061	2.055	2.038	2.038	2.025
μ_{Fe}		3.868	4.105	4.255	4.330	4.490	4.718
$\Delta_{AF/FM}$ (meV)		–	–	−58	−55	−57	42

The last row lists the energy difference between the anti-ferromagnetic and ferromagnetic structures ($\Delta_{AF/FM}=E_{AF}-E_{FM}$).

energies. Focusing now on the inorganic chains, a less-distorted octahedral geometry is observed for the FeO_6 entities compared to experiments. They show four nearly equivalent Fe-O bonds in their equatorial plane and two smaller apical Fe-O bonds, in agreement with a greater π-donor character for the hydroxyl ligands compared to the carboxylate ones. As a consequence of the more localised picture provided by the DFT+U formalism, the iron local magnetic moment slightly increases as a function of U_{eff}. It corresponds to the S=5/2 high-spin configuration, in agreement with the Fe^{III} oxidation state detected by Mössbauer spectroscopy measurements [9]. Note that within the LDA, the magnetic moments fall down to S=1/2 for U_{eff}<3.0 eV.

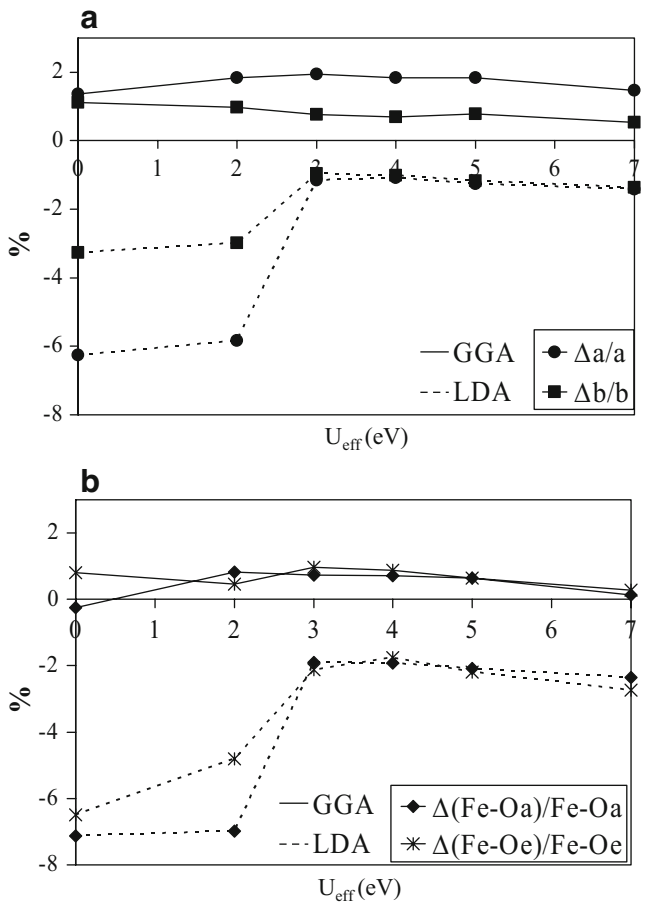

Fig. 2 Variations in % of **a** lattice parameters and **b** the Fe-O apical and equatorial bond distances computed with respect to experiments within the LDA+U and GGA+U approximations, as a function of U_{eff}

To seek for any long-range magnetic order, the energies of both the anti-ferromagnetic and the ferromagnetic structures were computed as a function of U_{eff}. As shown Table 1, the anti-ferromagnetic structure is favoured up to U_{eff}=7 eV lying a few k_BT lower than the ferromagnetic one. According to the literature, U_{eff} values lower than 5 eV should be used to properly account for iron oxides ground state properties [20]. The stabilisation of the ferromagnetic structure at larger U_{eff} (9 eV) should thus result from a too large localisation of the metallic 3d orbitals. This suggests weak anti-ferromagnetic interactions along the chains with a probable anti-ferromagnetic ordering at very low temperature. An insulating ground state is, therefore, expected for such an anti-ferromagnetic chain of high-spin Fe^{III} ions. This is supported by the density of states (DOS) of Fig. 3 in which the iron spin-up and spin-down contributions are given together with the ligand-type contribution. On this DOS, each band consists of opposite spins on the two iron atoms occurring along the chain, namely, Fe(1) and Fe(2). For these two atoms, a gap occurs between the spin-up/spin-down electronic states consistent with the high-spin configuration of the Fe^{III}. As a result of the 3d electron localisation that increases as a function of U_{eff}, the energy band gap also increases from U_{eff}=0 to 9 eV (note shown here), leading to a typical Mott–Hubbard insulating behaviour for low U_{eff} values and to a charge transfer insulating behaviour for larger U_{eff} values. As DFT is known to underestimate the optical gaps, the right U_{eff} value one should use in the calculations to properly

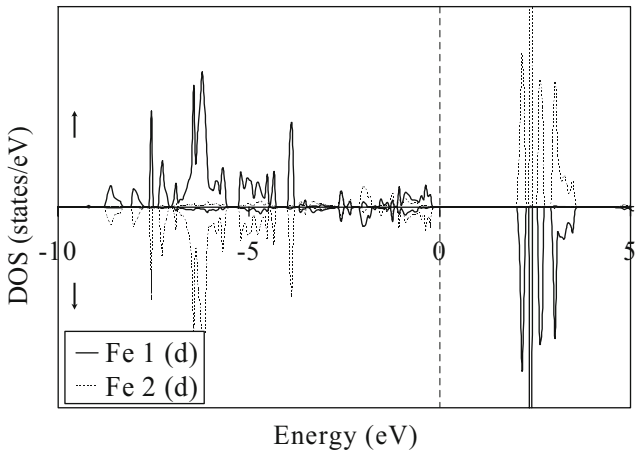

Fig. 3 Partial DOS projected on the Fe(1) and Fe(2) 3*d* orbitals for the neutral Fe{OH(BDC)} compound computed within the GGA+*U* approximation for U_{eff}=4 eV, using the Liechtenstein method (*J*= 1 eV). The positive and negative DOS correspond to the spin-up and spin-down DOS, respectively. The Fermi level is given by the *vertical dotted line*, as the zero reference energy

describe the electronic ground state of Fe{OH(BDC)} cannot be fairly determined here by simply comparing the experimental gaps to the computed ones. However, the redox properties of Fe{OH(BDC)} should not be drastically affected by the magnitude of these electronic gaps, as the nature of the first empty electronic bands does not change in the whole range of U_{eff}.

The electrochemical behaviour of Fe{OH(BDC)} was then investigated using the U_{eff}=4 eV recommended in the literature for iron oxides [20]. As a large number of lithium sites can be considered in the initial structure, we first started with the addition of extra electrons in the electronic structure of Fe{OH(BDC)}. As shown by the DOS of Fig. 3, one additional electron should fill half the first

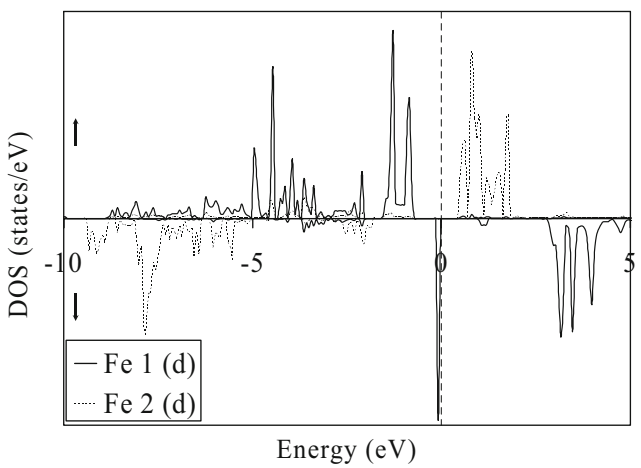

Fig. 4 Partial DOS projected on the Fe(1) and Fe(2) 3*d* orbitals for the reduced $Fe\{OH(BDC)\}^{-1/2}$ compound computed within the GGA+*U* approximation for U_{eff}=4 eV, using the Liechtenstein method (*J*=1 eV). The positive and negative DOS correspond to the spin-up and spin-down DOS, respectively. The Fermi level is given by the *vertical dotted line*, as the zero reference energy

empty band of Fe{OH(BDC)}. Because this band results from $Fe^{III}(5/2)$–$Fe^{III}(-5/2)$ anti-ferromagnetic interactions, no electronic de-localisation is expected along the chain for the additional electron. This is consistent with the spin-gap opening observed in the DOS of the reduced $Fe\{OH(BDC)\}^{-1/2}$ compound of Fig. 4 and with the localisation of the extra electron on every iron (see Fig. 5). A mixed-valence Fe^{III}/Fe^{II} state is, therefore, stabilised as Li is inserted into the starting material. Similar results are obtained when we added one Li^+ in the reduced $Fe\{OH(BDC)\}^{-1/2}$ compound. The mixed-valence state is associated with significant structural changes for the local Fe^{II} environment compared to the initial Fe^{III} one. The different sites considered in our calculations for Li insertion are illustrated by crosses on Fig. 1. When Li is inserted in site I, a significant Fe-OH bond elongation is observed in the relaxed crystal structure of $Li^{I}_{0.5}Fe\{OH(BDC)\}$ leading to alternating short and long Fe-OH bridges along the chain and to the formation of $(OH)^-$-Li^+. This local distortion results in a slight decrease of the *a*-lattice parameter and a larger increase of the *c*-lattice parameter (*a*=6.80 Å and *c*=7.30 Å), thus opening the channels of the MOF architecture. When Li is inserted in site II, a significant contraction of the channels is associated with the stabilisation of the Fe^{III}/Fe^{II} mixed-valence state. In particular, a significant decrease of the *c*-lattice parameter (*c*=6.40 Å) is observed for the $Li^{II}_{0.5}Fe\{OH(BDC)\}$ due to the interaction of Li^+ with the COO^- group, and to the formation of the $(O{=}C{-}O)^-$-Li^+. Such a distortion partially destroys the π-conjugation of the BDC linker, which is compensated by an efficient π-stacking interaction along the *c*-axis. Very close voltages are computed for the two insertion sites (V_I=2.50 V and V_{II}=2.52 V compared to *V*=2.7 V experimentally), in agreement with the similar DOS obtained for the $Li^{I}_{0.5}Fe\{OH(BDC)\}$ and $Li^{II}_{0.5}Fe\{OH(BDC)\}$ structures. Nevertheless, it seems unlikely that these two sites can be electrochemically achieved in the meantime, in particular, for

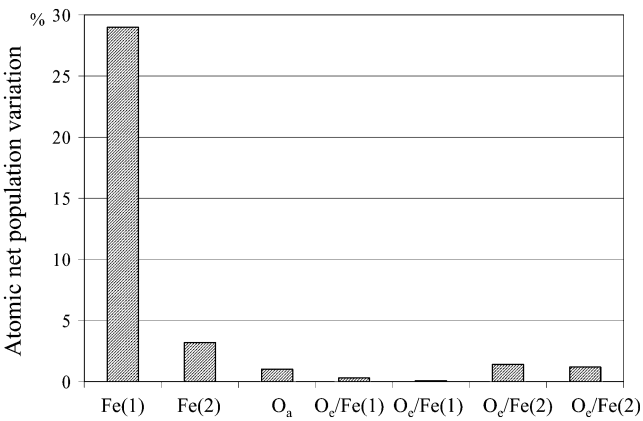

Fig. 5 Atomic net population analysis for the reduced $Fe\{OH(BDC)\}^{-1/2}$ compound computed within the GGA+*U* approximation for U_{eff}=4 eV, using the Liechtenstein method (*J*=1 eV)

they induce opposite structural breathing of the open channels. We are now undertaking the structural relaxations of various $Li^{i}Fe\{OH(BDC)\}$ (i=I/II, I/I, II/I) to check whether is it theoretically possible to insert more lithium in the structure. From an electronic point of view, we do not see any obvious reason to avoid further insertion as the spin-gap observed in the $Li_{0.5}Fe\{OH(BDC)\}$ structures is lower than that of the starting material. Nevertheless, under electrochemical conditions, some of the organic molecules present in the solvent can fill (at least partially) the open channels of the MOF. If these molecules were able to solvate and transport Li^+ into the structure, the kinetics of Li insertion should be favoured. However, a large c-lattice parameter should result from the insertion of these molecules, thus lowering the thermodynamical stability of site II. At this stage, it is thus tempting to correlate this kinetics/thermodynamics competition to the small capacity of the Fe{OH(BDC)} compound.

Conclusion

In the present study, we have shown that Fe{OH(BDC)} is a charge transfer or a Mott–Hubbard anti-ferromagnetic insulator, described by chains of iron ions in the (S=5/2) high-spin state, in agreement with Mössbauer spectroscopy. Very close structural parameters are obtained whatever the U_{eff} parameter used in the GGA+U calculations from the DFT limit (U=0 eV) to the strongly correlated limit (U_{eff}=9 eV) showing that the crystal structure is not governed by the electron correlation. The proper Fe^{III} S=5/2 spin configuration is obtained from U_{eff}=3 eV in the LDA+U calculations and for any U_{eff} values in the GGA+U calculations, in agreement with the more delocalised picture provided by the local density approximation. Each of the crystallographic sites considered in the calculations as possible Li insertion sites for the reduced $Li_{0.5}Fe\{OH(BDC)\}$ compound leads to the stabilisation of a localised Fe^{III}/Fe^{II} mixed-valence state along the inorganic chains. A spin-Peierls-like phase transition is likely to be the origin of this mixed-valence state, resulting in a spin-gap opening in the electronic band structure due to local structural distortions around the $Fe^{II}O_6$ monomers. Whether Li^+ gets close to the hydroxyl bridge of the inorganic chains or to the carboxylate group of the organic linkers, very different structural changes are observed in the reduced $Li_{0.5}Fe\{OH(BDC)\}$ relaxed structures. They correspond to opposite breathings of the MOF open channels, suggesting that all Li sites could not be reached under normal electrochemical conditions. An interesting outlook of this work would be to check the influence of the solvent used in the electrochemical cells on the Li content inserted into the MOF structures. Other alternatives to bypass the limited capacity of Fe{OH(BDC)} could also be found in replacing iron by lower 3d-filled transition metal or in decreasing the π-donor character of the in-chain bridging ligands. This should open new routes for the design of hybrid compounds with tuneable redox properties.

Acknowledgements We would like to thank Prof. Jean-Marie Tarascon, Prof. Gérard Ferey and the people from their group for sharing their experimental results. This work was supported by the French computational resources centres IDRIS and CINES (Contract Nos. 71750 and 09-11750) for the computations and by the Agence Nationale de le Recherche (Contract ANR-06-BLAN-0202).

References

1. James SL (2003) Chem Soc Rev 32:276
2. Rowsell JLC, Millward AR, Park KS, Yaghi OM (2004) J Am Chem Soc 126:5666
3. Janiak CJ (2003) J Chem Soc Dalton Trans 2781
4. Wang L, Tseng KK (2003) J Mater Chem 38:3019
5. Yaghi OM, O'Keeffe M, Ockwig NW, Chae HK, Eddaoudi M, Kim J (2003) Nature 423:705
6. Cussen EJ, Claridge JB, Rosseinsky MJ, Kepert CJ (2002) J Am Chem Soc 124:9574
7. Millange F, Serre C, Ferey G (2002) Chem Commun 822
8. Li X, Cheng F, Zhang S, Chen J (2006) J Power Sources 160:542
9. Férey G, Millange F, Morcrette M, Serre C, Doublet M-L, Grenèche J-M, Tarascon J-M (2007) Angew Chem 46:3259
10. Julien C, Gastro-Garcia SJ (2001) Power Sources 97/98:290
11. Padhi AK, Nanjundaswamy KS, Goodenough JB (1997) J Electrochem Soc 144:1188
12. Aydinol MK, Kohan AF, Ceder G, Cho K, Joannopoulo J (1997) Phys Rev B 56:1356
13. Mishra SK, Ceder G (1999) Phys Rev B 59:6120
14. Gillot F, Bichat MP, Favier F, Morcrette M, Doublet M-L, Monconduit L (2004) Electrochim Acta 49:2325
15. Bichat MP, Gillot F, Monconduit L, Favier F, Morcrette M, Lemoigno F, Doublet M-L (2004) Chem Mater 16:1002
16. Anisimov VI, Zaanen J, Andersen OK (1991) Phys Rev B 44:943
17. Anisimov VI, Aryasestiawan V, Liechtenstein AI (1997) J Phys Chem B Condens Mates Surf Interfaces Biophys 9:767
18. Wang L, Maxisch T, Ceder G (2006) Phys Rev B 73:195107
19. Persson K, Ceder G, Morgan D (2006) Phys Rev B 73:115201
20. Zhou F, Cococcioni M, Marianetti CA, Morgan D, Ceder G (2004) Phys Rev B 70:235121
21. Loschen C, Carrasco J, Neyman KM, Illas F (2007) Phys Rev B 75:035115
22. Kresse G, Furthmuller J (1996) Phys Rev B 54:11169
23. Kresse G, Furthmuller J (1996) Comput Mater Sci 6:15
24. Liechtenstein AI, Anisimov VI, Zaane J (1995) Phys Rev B 52: R5467
25. Perdew JP, Zunger A (1981) Phys Rev B 23:5048
26. Perdew JP, Burke S, Ernzerhof M (1996) Phys Rev Lett 77:3865
27. Perdew JP, Burke K, Wang Y (1996) Phys Rev B 54:16533
28. Kresse G, Joubert D (1999) Phys Rev B 59:1758